J Solid State Electrochem (2007) 11:1229–1238
DOI 10.1007/s10008-007-0274-8

ORIGINAL PAPER

Investigation of Pt–Ru nanoparticle catalysts for low temperature methanol electro-oxidation

G. Garcia · V. Baglio · A. Stassi · E. Pastor · V. Antonucci · A. S. Aricò

Received: 20 July 2006 / Revised: 15 December 2006 / Accepted: 11 January 2007 / Published online: 7 February 2007

Abstract Pt–Ru nanoparticle-based methanol electro-oxidation catalysts with high concentration of metallic phase on carbon black have been synthesised by a low-temperature colloidal preparation route. Amorphous Pt–Ru oxide nanoparticles were deposited on carbon and subsequently reduced in hydrogen stream at different temperatures to obtain crystalline phases with tailored particle size. The electro-catalytic activity for methanol oxidation was investigated in half-cell from 30 to 60 °C. The results were interpreted in terms of particle size, crystallographic structure, degree of alloying and carbon monoxide adsorption properties. The best performance was achieved for the catalyst with intermediate particle size in the investigated range. Furthermore, it is observed that the optimal properties for these catalysts depend on the operating temperature.

Keywords Pt–Ru catalysts · Methanol electro-oxidation · DMFCs · Particle size

G. Garcia · E. Pastor
Departamento de Quimica Fisica,
Universidad de La Laguna,
38071 La Laguna, Spain

V. Baglio · A. Stassi · V. Antonucci · A. S. Aricò (✉)
CNR-ITAE,
Via Salita S. Lucia sopra Contesse 5,
98126 Messina, Italy
e-mail: arico@itae.cnr.it

Introduction

Direct methanol fuel cells (DMFCs) are attractive devices to convert chemical energy into electrical energy, but their performance is limited by various drawbacks, including kinetic constraints and methanol cross-over from the anode to the cathode side through the membrane [1, 2]. In particular, the poor kinetics of the anode are a key problem in DMFC. To improve the efficiency of DMFCs, anode catalysts, which combine a high activity for methanol dehydrogenation and an improved tolerance towards CO poisoning, are required. At present, Pt–Ru alloys are the most active electro-catalysts for methanol oxidation [1]. The intrinsic catalyst activity, however, depends on the composition of the alloy particles; furthermore, the surface area plays a relevant role in enhancing the anode performance [3]. The electro-catalytic properties of Pt–Ru catalysts have been widely studied in the last four decades for DMFC applications [1]. Yet, limited attention was focused on the investigation of the optimal particle size for the electrochemical oxidation of methanol, in particular when small Pt–Ru nanoparticles (<3 nm) are employed [4]. On the contrary, large efforts have been addressed to investigate the effect of bi-metallic catalysts composition. As widely known, a significant particle size effect is present for the oxygen reduction process at Pt/C electro-catalysts [5]. It is widely recognised that nanostructured fuel cell catalysts are characterised by unique properties endowed by the effect of spatial confinement of Pt sites because of the small particle size and strong contribution of the surface to the overall behaviour [6].

In this work, an attempt to correlate the electrochemical behaviour of Pt–Ru catalysts to the particle size and, thus,

to the surface area was carried out. Different Pt–Ru/C catalysts with crystalline structures and amorphous, varying by the particle dimensions, were prepared and physico-chemically characterised.

Experimental

Preparation of catalysts

Four carbon-supported Pt–Ru catalysts for methanol oxidation with different particle size have been selected. All of them were 85% Pt–Ru (1:1)/Vulcan XC 72 and were prepared in-house by the sulphite complex route [7]. This consists of the following steps: (1) sulphite complexes of Pt and Ru, in appropriate amounts, were decomposed by hydrogen peroxide to form aqueous colloidal solutions of Pt and Ru oxides; (2) then, these particles were adsorbed onto a carbon black to form an 85% Pt–RuOx/Vulcan XC 72 catalyst; (3) finally, the amorphous oxides on carbon were reduced in a hydrogen stream at different temperatures to form a metallic alloy with different particle size.

Electrochemical experiments

For electrochemical measurements, the working electrodes were prepared with these catalysts according to the procedure described in a previous paper [8]. They consisted of carbon cloth, diffusion and catalytic layers with a Pt loading of 2 mg cm^{-2} and a geometric area of 0.5 cm^2. The carbon cloth was used as mechanical support for the diffusion and catalyst layers and as current collector. An interlayer composed of 80% wt. carbon black and 20% wt. polytetrafluoroethylene (PTFE) was deposited onto one side of carbon cloth to provide uniform diffusion pathways for the reactant molecules to the catalytic sites. A composite catalytic layer made of catalyst (85% wt.) and perfluoro-sulphonic acid ionomer (Nafion, 15% wt.) was deposited onto the diffusion layer; the catalytic layer forms an extended reaction zone with both electronic and ionic percolations within the layer. The electrode fabrication procedure was similar to that previously adopted for high-temperature DMFCs. No attempt was made to optimize the electrode structure for low-temperature application, e.g. by enhancing hydrophobic properties to favour CO_2 removal, being outside the scope of this work. A high surface area carbon (1,000 m^2 g^{-1} KETJEN BLACK) supported on a carbon cloth was used as the counter electrode, and a Hg/$HgSO_4$ reference electrode was connected to the electrochemical cell through a Luggin capillary whose tip was placed 0.5 mm distant from the working electrode surface. However, all potentials in the text are referenced to a reversible hydrogen electrode (RHE).

The potentiodynamic polarisation measurements were carried out in 1.0 M CH_3OH+0.1 M H_2SO_4 solution using a scan rate of 0.002 V s^{-1}. All the curves started at the open circuit potential (OCP), and the upper potential was limited to 0.85 V. As before, these experiments were carried out at 30, 40, 50 and 60 °C.

Solutions were prepared from bi-distilled water (CARLO ERBA) and analytical grade reagents. The working solution was 1.0 M methanol (99.9% CARLO ERBA) in 0.1 M sulphuric acid (98% ALDRICH) to simulate the behaviour of the catalyst in a typical DMFC. All electrochemical measurements were performed using a PGSTAT30 potentiostat (AUTOLAB), in an electrochemical cell using a three-electrode assembly.

Cyclic voltammograms (CVs) for methanol oxidation were recorded in the working solution between 0.00 and 0.85 V_{RHE} at a scan rate of 0.02 V s^{-1}.

Carbon-monoxide-stripping procedure was performed by first adsorbing CO at 0.10 V_{RHE} at two different temperatures (25 and 60 °C) for 30 min followed by flushing with He for 30 min while maintaining the potential at 0.10 V_{RHE}. According to the literature [4], this procedure allows to reach a saturation condition (monolayer) for the adsorbed CO. Afterwards, the potential was scanned from 0.1 to 0.75 V_{RHE} with a scan rate of 0.02 V s^{-1}.

Chronoamperometric curves were acquired in the working solution. The curves started from the OCP to a constant potential of 0.40 V_{RHE} for approximately 800 s. The experiments were carried out at four temperatures (30, 40, 50 and 60 °C).

Physico-chemical characterisation of catalysts and electrodes

X-ray diffraction (XRD) patterns for powder catalysts and electrodes (before and after electrochemical experiments) were recorded with a Philips X′Pert X-Ray diffractometer using a $Cu-K_\alpha$ source operating at 40 kV and 30 mA. The two-theta scale was calibrated by using a standard silicon reference (Panalytical). The peak profiles of the (2 2 0) reflection for the face-centred-cubic (fcc) structure of Pt–Ru phase were obtained by applying the Marquardt algorithm [9]. Instrumental broadening was determined by using a standard platinum sample. The alloy composition was determined from the XRD peaks by using a calibration curve obtained for bulk alloys [10]. X-ray fluorescence (XRF) analysis of the catalysts was carried out with a Bruker AXS S4 Explorer spectrometer operating at 1 kW and equipped with a Rh X-ray source, a LiF 220 crystal analyser and a 0.12° divergence collimator. The Pt/Ru atomic ratio was determined with the $Pt-L_\alpha$ and $Ru-L_\alpha$ emission lines after appropriate calibration with standard samples.

Results

Physico-chemical analysis

The atomic ratio between Pt and Ru was 1:1 for all catalysts. The concentration of the metallic phase on carbon was 85% wt.; this was confirmed by XRF analysis. XRD results of carbon-supported catalysts (powder, electrodes before and after electrochemical measurements) showed, for most samples, the cubic fcc crystallographic structure of the Pt–Ru alloy (Fig. 1). In the case of the amorphous Pt–Ru oxide (Table 1), the broad peaks recorded in the X-ray pattern are not associated to any PtOx or RuOx structure. They reflect the X-ray scattering of a disordered material. The crystallographic parameters have been calculated from the formula [3, 10]:

$$a_{\mathrm{fcc}} = \frac{\sqrt{2} \cdot \lambda_{\mathrm{K}\alpha 1}}{\sin \theta_{\max}} \tag{1}$$

where a_{fcc} is the lattice dimension of the fcc structure, λ is the wavelength of the X-ray source, $\theta_{\max}$ is the Bragg angle.

The degree of alloying was calculated according to the empirical relationship described in [10]:

$$a_{\mathrm{fcc}} = 3.8013 + 0.1249\, X_{\mathrm{Pt}} \tag{2}$$

where X_{Pt} is the atomic fraction of Platinum in the Pt–Ru alloy.

The mean particle size (L) was determined by the Debye-Sherrer Eq. 3:

$$L = \frac{0.9 \cdot \lambda_{\mathrm{K}\alpha 1}}{B_{2\theta} \cdot \cos \theta_{\max}} \tag{3}$$

where B is the true particle size broadening as determined from the 220 reflection full width at half maximum corrected by the instrumental broadening (standard sintered Pt foil) [3]:

$$B_{2\theta} = \sqrt{B_{2\theta\,\mathrm{measured}} - B_{2\theta\,\mathrm{instrument}}} \tag{4}$$

These physico-chemical parameters are reported in Table 1. The particle size (typically a few nanometres), appears to increase slightly after the preparation of the electrodes for all catalysts, but no significant change is observed after electrochemical experiments. A clear estimation of the particle size from XRD after the electrode preparation was not possible because of the interference of the X-ray scattering from carbon cloth, PTFE and Nafion. This made an univocal determination of the X-ray pattern base line difficult. The high concentration of Pt–Ru particles on the carbon support does not allow to estimate particle size from transmission electron microscopy (TEM) exactly. Accordingly, we have made reference to the particle size in the raw powder. Except for the amorphous oxide, particle size of 1.6, 2.2 and 2.6 nm were obtained for Pt–Ru in the powder catalysts from XRD. This analysis also shows a slight change of the alloy composition during the preparation of powder catalysts. Both Pt and Ru are present in an amorphous form before the reduction process. Although all the catalysts have the same nominal Pt/Ru ratio equal to 1, the different reduction procedure may cause that some amount of Ru remains amorphous determining different degree of alloying (alloy composition) as derived from the shift of diffraction peaks. An increase of the Ru content in the Pt–Ru alloy as detected from XRD is observed as long as the particle size increases; this is a consequence of a strong reduction treatment (Table 1). Such an evidence indicates that the reduction process with hydrogen favours the formation of a solid solution with increasing content of Ru atoms in the Pt fcc

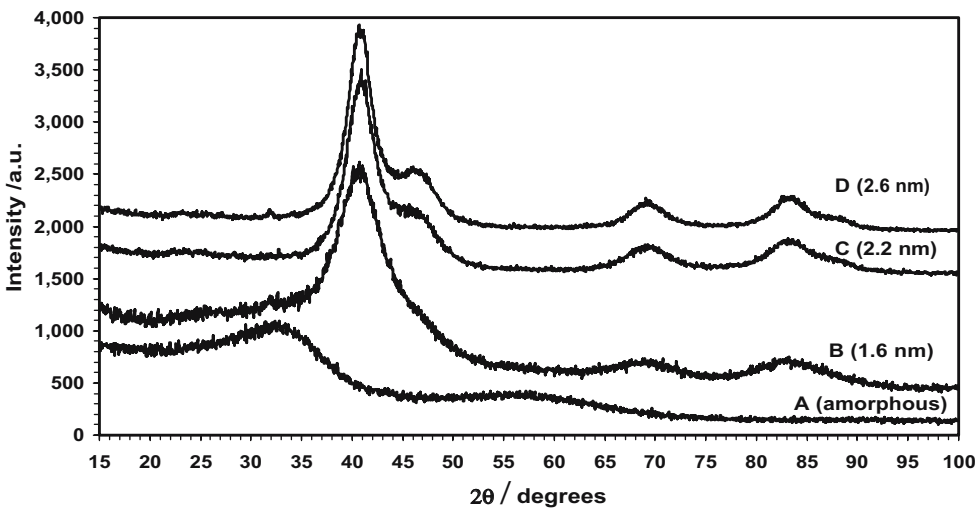

Fig. 1 XRD patterns of 85% Pt–Ru/C catalysts

Table 1 Alloy composition and particle size as derived by XRD

Catalyst batch	Composition	Peak position/ 2θ deg (CuKα) 220 reflection	Lattice parameter (nm)	Density PtRu alloy (g cm^{-3})	Powder particle size (nm)	Pt(%) in the alloy	Ru (%) in the alloy
A	85% (Ru–Pt)Ox/C	–	–	–	1.3[a]	52	48
B	85% Ru–Pt/C	68.836	0.386	17.1	1.6	48	52
C	85% Ru–Pt/C	69.132	0.384	17.3	2.2	33	67
D	85% Ru–Pt/C	69.133	0.384	17.3	2.6	33	67

[a] TEM analysis

structure. The atomic radius of Ru is slightly smaller than Pt, i.e. 0.133 vs. 0.139 nm, respectively; metallic Ru crystallises in the hexagonal structure (JCPDS 60–663), whereas, Platinum in the cubic structure (JCPDS 40–802). The PtRu alloy in our catalysts has the fcc structure. Interestingly, the crystalline alloy composition for the catalysts with larger particle size as derived from XRD indicates an excess of Ru with respect to the total composition derived from XRF (Pt/Ru atomic ratio equal to 1). Because no other crystalline phase related to PtOx or RuOx was identified in the XRD patterns and having used a calibration curve obtained with bulk alloys [10], it is derived that this curve could not be appropriate for nanoparticles. In fact, a shift towards higher Bragg angles was already observed for pure Pt nanoparticles highly dispersed on a carbon support [11]. Alternatively, because the extent of reduction of amorphous metal oxides and, thus, the depth of reduced metallic shell layer above the oxide core depends on both temperature and time of reduction, an oxide core of variable composition may remain beneath of the metallic shell not easily detected by XRD.

TEM images of the catalysts (Fig. 2a) indicate a high degree of agglomeration because of the high concentration of metal particles on carbon. TEM analysis confirms the increase in particle size of the active phase in the electrodes (Fig. 2b) with respect to the raw powder previously observed from XRD. Moreover, particle size of the amorphous oxide catalyst can be obtained, and a value of about 1.3 nm is determined for the powder and 1.5 nm for the electrode.

Cyclic voltammetry

A comparison of the voltammetric profiles for the Pt–Ru/C catalysts at a sweep rate of 0.02 V s^{-1}, in the working solution at 30 and 50 °C, are given in Fig. 3. It is clearly observed that, as the temperature is increased, the onset potential for the oxidation of methanol shifts negatively and the oxidation current increases for each catalyst. At the highest temperature, the onset of methanol oxidation during the forward sweep is approximately 0.30 V vs. RHE for A (1.3 nm) and D (2.6 nm) catalysts, whereas for the B (1.6 nm) and C (2.2 nm) catalysts with intermediate particle size is about 0.25 V vs. RHE.

Comparing the behaviour of catalysts A–D, it is concluded that catalyst A with amorphous properties is the worst for methanol oxidation, possibly because of the significant amount of metal oxide that inhibits this reaction, especially the dehydrogenation [1]. Whereas catalyst D, characterised by a large particle size, especially in the electrode form (see Fig. 2b), develops very low currents, only slightly higher than the amorphous oxide. Finally, the best catalysts for methanol oxidation were B and C catalysts with particle size of 1.6 and 2.2 nm, as it is seen in Fig. 3. Accordingly, the intermediate particle size appears to be the most appropriate solution because of the presence of both a well-defined fcc crystalline structure (with respect to the amorphous sample) and higher number of catalytic sites with respect to the catalyst composed of big particles.

The electro-oxidation of methanol on Pt–Ru catalysts proceeds through the mechanism (sequence of non-elementary reaction steps) described below. First, a sequence of dehydrogenation steps gives rise to adsorbed methanolic residues, according to the following scheme [1]:

$$CH_3OH + Pt \rightarrow Pt - (CH_2OH)_{ads} + H^+ + 1\ e^- \quad (5)$$

$$Pt - (CH_2OH)_{ads} + Pt \rightarrow Pt_2 - (CHOH)_{ads} + H^+ + 1\ e^- \quad (6)$$

$$Pt_2 - (CHOH)_{ads} + Pt \rightarrow Pt_3 - (CHO)_{ads} + H^+ + 1\ e^- \quad (7)$$

A surface rearrangement of the methanol oxidation intermediates gives carbon monoxide, linearly or bridge bonded to Pt sites, as following:

$$PtCHO \rightarrow Pt - C \equiv O + H^+ + 1e^- \quad (8)$$

or

$$PtCHO + Pt \rightarrow \begin{matrix} Pt \\ Pt \end{matrix} > C = O + H^+ + 1e^- \quad (9)$$

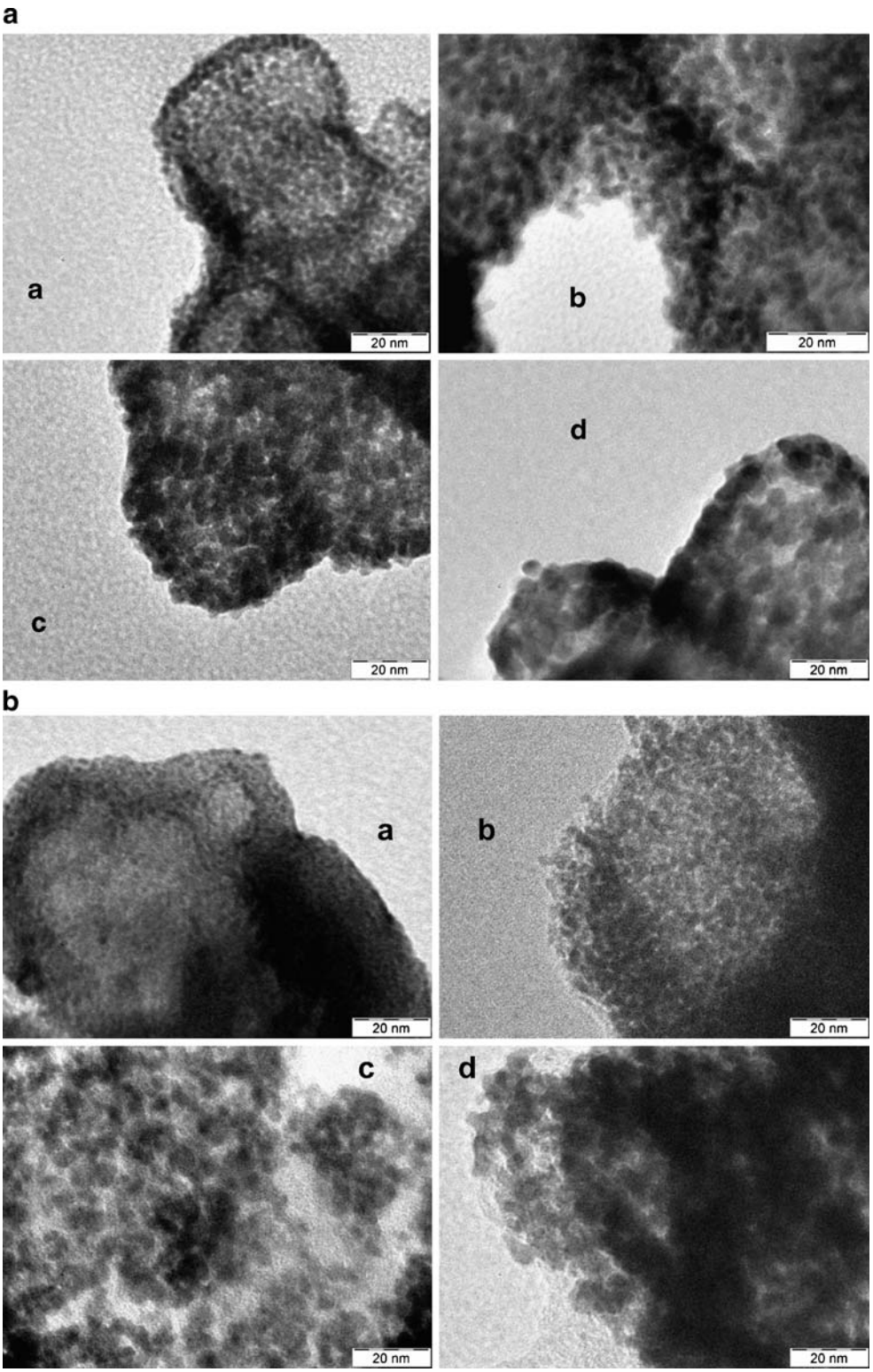

Fig. 2 **a** TEM micrographs of *A* amorphous, *B* 1.6 nm, *C* 2.2 nm and *D* 2.6 nm Pt–Ru/C catalysts. **b** TEM micrographs of Pt–Ru/C catalysts after electrode preparation. *A*, *B*, *C* and *D* refer to the catalysts reported in Table 1

At suitable electrode potentials (0.2 V vs. RHE), water discharging occurs on Ru sites with formation of Ru–OH groups at the catalyst surface [1, 4]:

$$Ru + H_2O \rightarrow Ru - OH + H^+ + 1e^- \quad (10)$$

The final step is the reaction of Ru–OH groups with neighbouring methanolic residues adsorbed on Pt to give carbon dioxide (bifunctional mechanism):

$$Ru - OH + Pt - CO \rightarrow Ru + Pt + CO_2 + H^+ + 1e^- \quad (11)$$

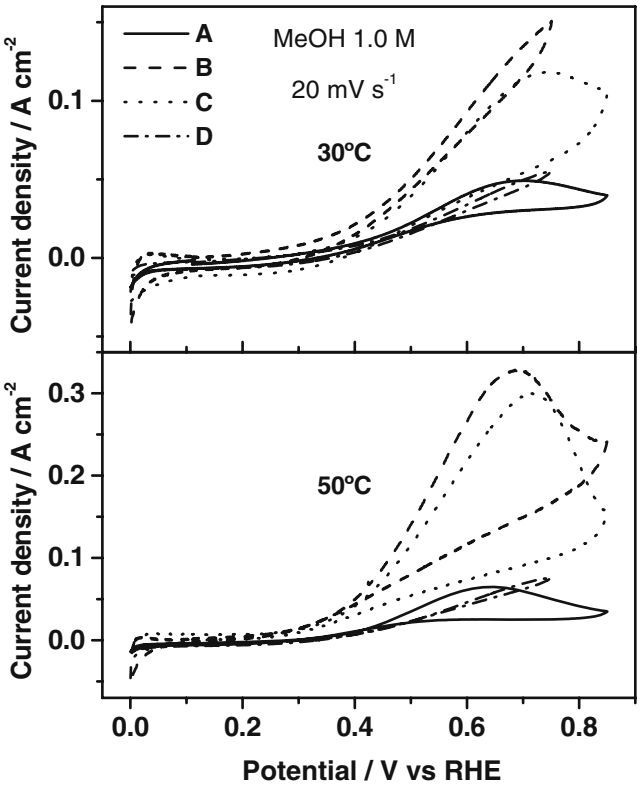

Fig. 3 Voltammetric profiles for the Pt–Ru/C catalysts at a sweep rate of 0.02 Vs^{-1} in 1 M methanol and 0.1 M H_2SO_4 solution at 30 and 50 °C

The rate-determining step (rds) for methanol oxidation at PtRu catalysts at medium temperatures (60 °C) is usually associated with CO removal, whereas at room temperature, the initial dehydrogenation process also plays a significant role [1, 4].

Stationary measurements

Stationary chronoamperometric curves were measured at 0.4 V vs. RHE (this potential represents a typical operating condition of a low-temperature DMFC anode) at different temperatures (Fig. 4). In all cases, the stationary current increases with the temperature; in the case of catalysts A (1.3 nm) and D (2.6 nm), the performance is poor; for all catalysts, even at 60 °C, a slight decay is always present. The catalyst A exhibits very low stationary current for methanol oxidation below 50 °C (not shown); at 60 °C, the current is comparable to the D catalyst. The best catalysts for the oxidation of methanol at this potential are B and C, in agreement with the voltammetric studies. For $T<50$ °C, the best performance is achieved with catalyst B (1.6 nm), whereas for $T=60$ °C, catalyst C (2.2 nm) shows higher currents (the current is similar for both catalysts at 50 °C). This indicates that the effect of active surface area that is larger for catalyst B than C (see "Polarisation experiments") is prevailing at low temperatures provided that the structure is crystalline.

Assuming that PtRu particles have a spherical shape as derived from TEM and that the degree of agglomeration is similar for all the catalysts, the correlation between the metal surface area (MSA) and XRD-derived particle size is [12]:

$$\mathrm{MSA} = 6 \cdot 10^4 / (\rho \cdot d) \tag{12}$$

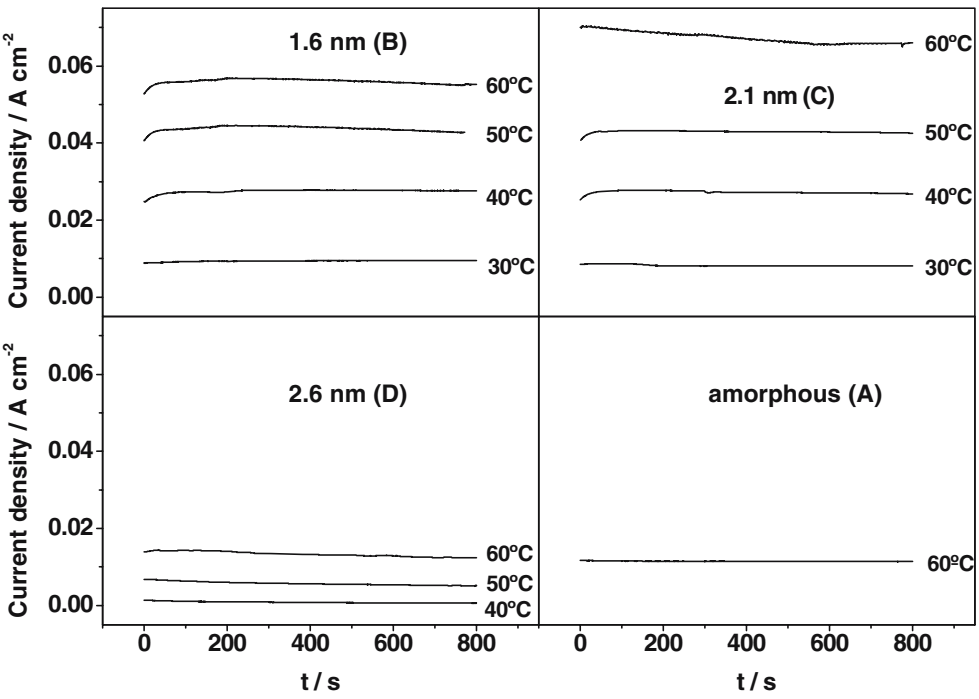

Fig. 4 Chronoamperometric curves measured at 0.4 V vs. RHE for the Pt–Ru/C catalysts at different temperatures

where ρ (g cm^{-3}) is the density of Pt–Ru alloy and d (Å) is the average particle size. The ρ values for each composition are derived from XRD data as follows [12]:

$$\rho = \text{Unit cell weight} \Big/ \text{Unit cell volume} = 4 \times 10^{24}((X_{\mathrm{Pt}}\mathrm{FW}_{\mathrm{Pt}})+(X_{\mathrm{Ru}}\mathrm{FW}_{\mathrm{Ru}})) \Big/ \left((a_{\mathrm{fcc}})^3 N_{\mathrm{A}}\right) \quad (13)$$

where X_{Pt} and X_{Ru} are the atomic fractions of Pt and Ru, $\mathrm{FW}_{\mathrm{Pt}}$ and $\mathrm{FW}_{\mathrm{Ru}}$ are the formula weights (g mol.$^{-1}$) of Pt and Ru, a_{fcc} (Å) is the lattice parameter, N_{A} (mol^{-1}) is the Avogadro number.

According to this formula, the maximum theoretical surface area increases as the mean particle size and the density ρ decrease. As the density is quite similar for the catalysts (Table 1), the surface area of the catalyst B is higher than catalyst C as further confirmed by CO-stripping experiments (see "CO stripping").

Polarisation experiments

Polarisation curves for the electrochemical oxidation of 1 M methanol in the working solution at 30, 40, 50 and 60 °C for the four different catalysts are shown in Fig. 5. The experiments start from the OCP in the positive scan direction up to 0.6 V at 0.002 V s^{-1}. Also in this case, an activation effect of the temperature is observed. From Fig. 5, it is also possible to establish the catalyst with the highest catalytic activity at different temperatures. In the potential range studied, catalyst B (1.6 nm) is the best for temperatures below 50 °C, whereas the largest current above 50 °C is obtained with catalyst C (2.2 nm). Again, catalysts A (1.3 nm) and D (2.6 nm) present a very low activity towards methanol oxidation. These results are in agreement with those obtained with cyclic voltammetry and chronoamperometry.

The analysis of temperature effect is investigated in the Arrhenius plot (log I vs. $1/T$) at 0.45 V vs. RHE (Fig. 6). This potential was selected because there was no significant oxidation current for the amorphous catalyst at 0.4 V (RHE). The curves show an increase of the current density over the whole temperature range for all the catalysts. The slope is similar with the exception of catalyst B, indicating a lower activation energy.

Figure 6 shows that the activation energy is high for catalyst A (amorphous) and becomes much lower for metallic catalysts where, however, it strongly increases with particle size and possibly with Ru enrichment. It is well known that the methanol and CO oxidation processes are structure-sensitive reactions [1]. Wieckowski et al. [13] showed for Pt–Ru surfaces that the catalytic activity is maximised on (111) crystallographic planes, and it decreases for high Miller index planes as well as in the presence of lattice defects. The small activation energy for the crystalline catalyst B compared to the amorphous catalyst A is possibly due to the absence of crystallographic order in this latter. Yet, the increase of the Ru content in the alloy possibly limits the dehydrogenation of methanol that is favoured by the presence of three neighbouring Pt sites; thus, the activation energy increases as the Ru content in the crystalline alloy increases.

CO stripping

In the low-temperature range, two reaction steps significantly influence the methanol oxidation, i.e. dehydrogena-

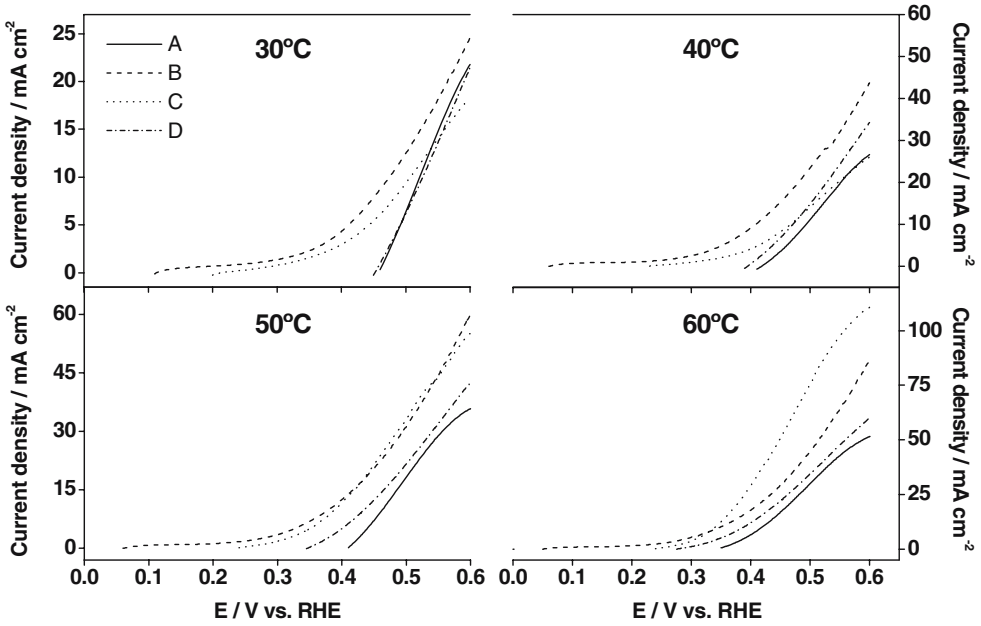

Fig. 5 Polarization curves for the electrochemical oxidation of 1 M methanol at 30, 40, 50 and 60 °C for the four different Pt–Ru/C catalysts

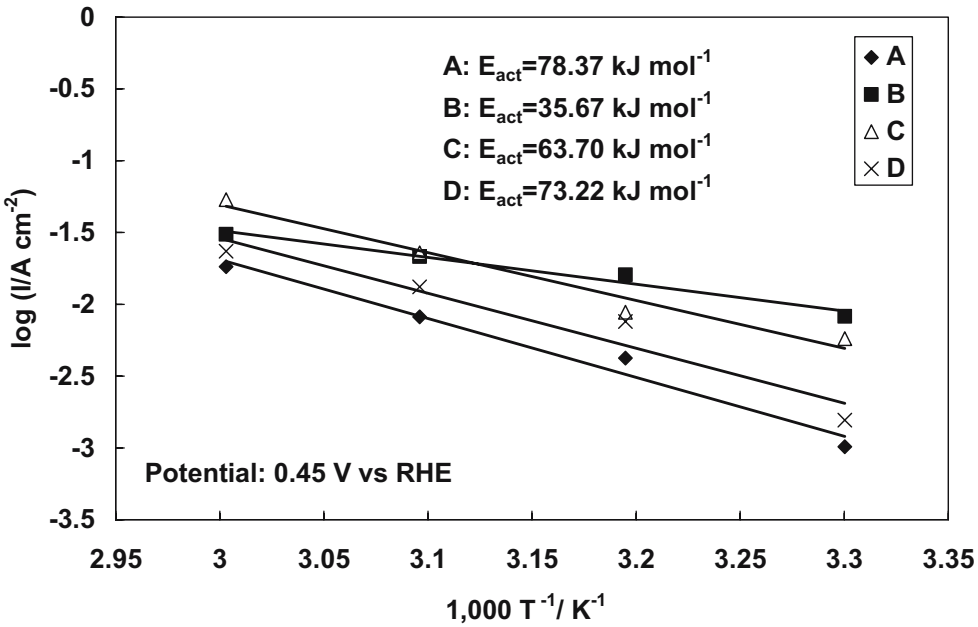

Fig. 6 Arrhenius plot and activation energies at 0.45 V vs. RHE for the different Pt–Ru/C catalysts

tion and carbon monoxide removal [1]. To get better insights on how the methanol oxidation is related to carbon monoxide removal, CO stripping was investigated for the most-performing catalysts (B and C) with intermediate particle size (Fig. 7). The stripping profile for both catalysts is similar at 25 °C; the onset potential for the oxidation is observed at about 0.35 V and the peak potential around 0.48 V vs. RHE. However, at 60 °C, the CO-stripping profiles differ significantly. Firstly, the stripping peak potentials for both catalysts are shifted to more negative potentials with respect to 25 °C. In the case of catalyst C (2.2 nm), a well-defined peak is observed at 0.38 V vs. RHE, whereas for catalyst B, a broader and smaller CO-stripping peak appears at around 0.43 V vs. RHE. The amount of adsorbed CO is significantly larger for the catalyst with 2.2 nm particle size that shows a well-defined fcc structure than the sample with smaller (1.6 nm) particle size, characterised by lower shift of reflections in the XRD pattern. Furthermore, at 60 °C, a significant decrease in the amount of adsorbed CO is recorded for the catalyst B with respect to 25 °C. The XRD pattern of the latter sample shows a clear evidence of crystalline structure, but the structure is not well defined as in the catalysts C and D with larger particle size. Possibly, the surface arrangement of atoms in this catalyst is that of the fcc crystallographic structure but the spatial confinement and chemical properties may significantly differ from catalysts C and D. Catalyst B results in a compromise between crystalline structure and amorphous properties that are derived from the surface contribution (more than 50% of the atoms in each particle are located on the surface). This may cause the small activation energy observed above ("Polarisation experiments"). On the other hand, the large activation energy recorded in the amorphous catalyst ("Polarisation experiments") is derived from the absence of a proper surface arrangement of catalytic sites.

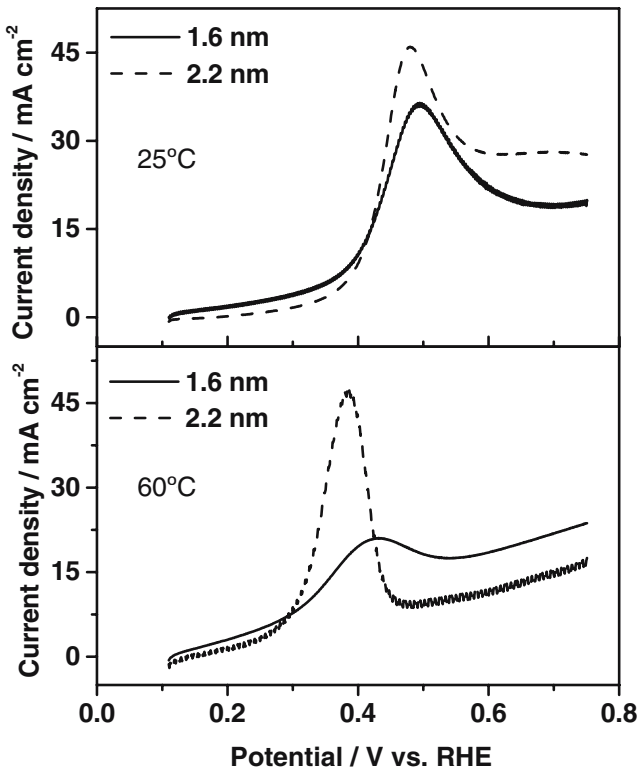

Fig. 7 CO stripping analysis for catalysts B (1.6 nm) and C (2.2 nm) at 25 and 60 °C

The above results indicate that CO adsorption may be significantly influenced by the temperature, the size of the Pt–Ru particles, etc. Generally, the CO adsorption on Pt is quite a irreversible process at low temperatures with the

onset of CO desorption appearing only at 120 °C [14]. Conventional Pt–Ru catalysts show a significantly larger degree of CO tolerance than Pt at lower temperatures (80 °C). Possibly, Pt–Ru catalysts in the low particle size range adsorb lower amount of CO mainly because of the fact that surface sites are generally more oxidised being the thermal reduction in hydrogen carried out under mild conditions. This would reflect an increase of CO tolerance but lower capability to adsorb methanolic residues (CO-like species) that are reaction intermediates in the methanol oxidation process. This would not favour the methanol oxidation at high temperatures on the catalyst with small particle size; whereas at 30 °C, the adsorption of CO-species on the catalyst with particle size of 1.6 nm is still quite effective, and it shows, at this temperature, good catalytic activity towards methanol oxidation as compared to the catalysts with lower particle size.

Assuming that at 25 °C the CO adsorption process on these catalysts approaches the saturation (monolayer) and taking into account a CO-stripping charge of 420 μC per real cm^2 of active surface, the corresponding active surface area is about 27 m^2/g and 23 m^2/g for the catalyst B and C, respectively. These values are smaller than the typical active surface area of the state-of-art fuel cell electrocatalysts (typically, 50 m^2/g for a Pt particle size of 3 nm and Pt loading in the electrode of about 0.5 mg cm^{-2} [14]). Possibly, the significant degree of agglomeration of the PtRu particles, the high metal loading and small triple-phase boundary significantly reduce the active surface area. Yet, it is confirmed that the smaller is the catalyst particle size the larger is the surface area for CO adsorption.

Discussion

The catalyst activities in increasing order for methanol oxidation show a maximum for a Pt–Ru particle size in the range between 1.6 and 2.2 nm, provided that the structure is crystalline; the catalyst with smaller particle size (1.6 nm) is more active below 50 °C; whereas, the catalyst with 2.2 nm particle size is more active at 60 °C. Amorphous catalysts show poor activity because of the absence of proper arrangements of atoms on the surface, being the methanol oxidation a structure-sensitive process. As the particle size increases above 2.2 nm, the loss of surface area causes a decrease of catalytic activity.

The differences in catalytic activity towards the methanol oxidation reaction may not only be related to the effect of particle size but also to the surface chemistry that can be different for the various catalysts. Generally, catalysts with smaller particle size are more oxidised on the surface, and it is well known that the presence of Pt and Ru oxides on the surface in the amorphous catalyst does not favour dehydrogenation [1].

With regard to the surface chemistry, the behaviour of the catalysts A–D can be thus summarised as follows:

Catalyst A (amorphous) shows poor catalytic activity because of significant content of oxides on its surface. This does not permit breaking of C–H bonds in methanol.

Catalyst B (1.6 nm) appears to have the highest efficiency for the methanol oxidation reaction at low temperatures. Possibly, the larger Pt content in the alloy allows an enhancement of methanol oxidation rate at low temperatures. It was pointed out before that three neighbouring Pt sites are necessary for methanol dehydrogenation. The initial dehydrogenation may be the rds at very low temperatures. Furthermore, the effect of strong spatial confinement and oxidation states on the surface (this catalyst was reduced under mild conditions with respect to catalysts C and D) determines an unusual behaviour towards CO adsorption with temperature. At high temperatures, water discharging on Ru sites limits the process much more significantly than the dehydrogenation step [1].

Catalyst C (2.2 nm) provides the best catalytic activity at higher temperatures (above 50 °C). It seems that the alloy composition more rich in Ru is responsible for the change in the catalytic properties. Structural effects may also determine this behaviour. As discussed above, the (111) crystallographic planes play the highest catalytic activity for the Pt–Ru single crystals [13, 15]. Accordingly, the fraction of these planes increases with the particle size, but simultaneously, the surface area decreases [5]. A particle size of 2.2 nm may represent a good compromise. CO-stripping studies indicate that, while the temperature increases, the onset potential for CO_{ads} oxidation shifts to negative values more significantly than catalyst B, and no significant changes in the CO coverage are observed.

Catalyst D (2.6 nm) is slightly better than the amorphous (A) catalyst but the catalytic activity is affected by the decrease in surface area, especially after membrane and electrode assembly preparation (see "TEM analysis"). Alternatively, it may be hypothesised as a speculative hypothesis that the higher reducing temperature for this catalyst may have induced surface enrichment in one of the two elements. As stated above, it is well known that methanol dehydrogenation occurs preferably at three neighbouring Pt sites [1, 16], and then if the surface is rich in Ru, insufficient sites are available for methanol oxidation. On the other hand, a large Pt content on the surface may cause a loss of catalytic activity because of the lack of bifunctional mechanism (see "Methanol oxidation mechanism," Eq. 11) that plays a major role in the methanol oxidation on Pt–Ru catalysts [16]. Unfortunately, conventional surface analysis, e.g. by X-ray photoelectron spectroscopy (XPS), does not permit an appropriate information on the surface composition for such small particles, as it also reflects the bulk properties. Typical analysis depth for

XPS experiments is about 5 nm, thus well above the particle size of the present catalysts. Ion-scattering techniques may be more appropriate. Furthermore, because various parameters govern the electro-catalytic behaviour, it is difficult to highlight clearly the role of particle size and alloy composition. It is necessary to tailor precisely the alloy composition to evaluate the effect of the particle size only or vice versa. Further studies could be addressed on this direction.

Conclusions

Carbon supported PtRu catalysts were prepared from the amorphous oxides (85% PtOx–RuOx/Vulcan XC 72) by reduction in a hydrogen stream to form metallic alloys with different particle size (1.6, 2.2 and 2.6 nm); the amorphous sample was also investigated for comparison. Methanol electro-oxidation appears to be promoted by the catalysts with intermediate particle size. This is attributed to a suitable compromise between crystalline properties and MSA. In the lower temperature range (<50 °C), the performance of the catalyst with 1.6 nm average particle size prevails probably because of a less-irreversible adsorption of CO-like reaction intermediates. The coverage of such species on this catalyst decreases at higher temperatures causing a decrease of the reaction rate that is generally proportional to the surface concentration of reaction intermediates. Accordingly, the catalyst with 2.2 nm average particle size gives rise to the best performance at temperatures higher than 50 °C. This indicates that appropriate tailoring of the particle size in the Pt–Ru catalysts could be advantageous for the specific application including low- or high-temperature DMFCs as well as reformate-air fuel cells.

Acknowledgements CNR-ITAE authors acknowledge the support from "Regione Piemonte" through the Micro Cell project (Delibera della Giunta Regionale n° 25-14654 del 31/01/05). Garcia thanks the MEC for a FPI grant.

References

1. Aricò AS, Srinivasan S, Antonucci V (2001) Fuel Cells 1:133
2. Pastor E, Wasmus S, Iwasita T, Arèvalo MC, Gonzalez S, Arvia AJ (1993) J Electroanal Chem 350:97
3. Radmilovic V, Gasteiger HA, Ross PN Jr (1995) J Catal 154:98
4. Ren X, Zelenay P, Thomas S, Davey J, Gottesfeld S (2000) J Power Sources 86:111
5. Kinoshita K (1990) J Electrochem Soc 137:845
6. Aricò AS, Bruce P, Scrosati B, Tarascon J-M, Van Schalkwijk W (2005) Nature Mater 4:366
7. Petrow HG, Allen RJ (1976) US Patent 3(992):331
8. Aricò AS, Baglio V, Di Blasi A, Modica E, Antonucci PL, Antonucci V (2003) J Electroanal Chem 557:167
9. Aricò AS, Creti P, Kim H, Mantegna R, Giordano N, Antonucci V (1996) J Electrochem Soc 142:3950
10. Gasteiger HA, Ross PN Jr, Cairns E (1993) J Surf Sci 67:293
11. Starz KA, Auer E, Lehmann T, Zuber R (1999) J Power Sources 84:167
12. Arico' AS, Antonucci PL, Modica E, Baglio V, Kim H, Antonucci V (2002) Electrochim Acta 47:3723
13. Chrzanowski W, Wieckowski A (1998) Langmuir 14:1967
14. Srinivasan S, Mosdale R, Stevens P, Yang C (1999) Annu Rev Energy Environ 24:281
15. Chrzanowski W, Kim H, Wieckowski A (1998) Catal Letters 50:69
16. Antolini E (2003) Mater Chem Phys 78:563